





RESEARCH ARTICLE

Measurements and scaling of buoyancy-induced flows in ventilated tunnels

Pietro Salizzoni^{1,2} , Cosimo Peruzzi^{1,*} , Massimo Marro¹ , Pietro Cingi^{1,3,4}, Diego Angeli^{3,4} , Thierry Kubwimana⁵ and Antoine Mos⁵

¹Laboratoire de Mécanique des Fluides et d'Acoustique (LMFA), UMR5509, Université de Lyon, Ecole Centrale de Lyon, CNRS, Université Claude Bernard Lyon 1, INSA Lyon, 36 Avenue Guy de Collonge, 69130 Ecully, France

²Department of Environmental, Land and Infrastructure Engineering (DIATI), Politecnico di Torino, Corso Duca degli Abruzzi 24, 10129 Turin, Italy

³Department of Sciences and Methods for Engineering (DISMI), University of Modena and Reggio Emilia, Via Amendola 2, 42122 Reggio Emilia, Italy

⁴Mimesis s.r.l., Via Contrada 309, 41125 Modena, Italy

⁵Centre d'Etudes des Tunnels (CETU), 25 Avenue Francois Mitterrand, 69500 Bron, France

*Corresponding author. E-mail: cosimo.peruzzi@ec-lyon.fr

Received: 28 June 2022; **Revised:** 15 February 2023; **Accepted:** 2 May 2023

Keywords: Plumes/thermals; Stratified turbulence; Mass exchangers; Laser-based flow diagnostics

Abstract

We investigate the ventilation conditions required to control the propagation of smoke, produced by a tunnel fire, in the presence of two inertial forcings: a transverse extraction system and a longitudinal flow. For that purpose, we performed a series of experiments in a reduced-scale tunnel, using a mixture of air and helium to simulate the release of hot smoke during a fire. Experiments were designed to focus on the ventilation flows that allow the buoyant release to be confined between two adjacent extraction vents. Different source conditions, in terms of density and velocity of the buoyant release, were analysed along with different vent configurations. Experiments allowed us to quantify the increase of the extraction velocity needed to confine the buoyant smoke, overcoming the effect of an imposed longitudinal velocity. Vents with a rectangular shape, and spanning over the whole tunnel width, provide the best performance. Finally, we studied the stratification conditions of the flow, individuating four regimes. Interestingly, when the stratification conditions fade out, as both the longitudinal flow and vertical extraction flows increase, the flow dynamics becomes almost independent of the forcing induced by the presence of buoyant smoke, which eventually acts as a passive scalar transported by the flow.

Impact Statement

Ventilation systems are a crucial aspect in preventing disastrous consequences following road tunnel car accidents. Their purpose is to control the smoke propagation, confining it in a limited area or pushing it away, thus allowing the tunnel users to safely escape. The correct performance of a ventilation system is dictated by different fluid dynamic forcings, i.e. the buoyancy induced by the tunnel fire, the pressure-gradient inertial force produced by meteorological effects on the tunnel entrances and the inertial forces created by the tunnel fans. The relative magnitude of these forcings has a direct impact on the ventilation configuration required to control the spreading of the fire smoke and its stratification within the tunnel. Therefore, we have performed flow visualisation experiments in a reduced-scale tunnel facility to identify the control parameters

that allow for the confinement of a buoyant release through a ventilation system equipped with longitudinal and transverse fans.

1. Introduction

Road tunnels, by their nature, are narrow and tubular semi-enclosed structures where the propagation of smoke and heat emitted by accidental fires is potentially difficult to control. On some dramatic occasions, the presence of a fire may induce temperatures rapidly exceeding 1000 °C and release a huge amount of harmful smoke, making the access of firefighters difficult or even impossible. For all these reasons, road accidents occurring within a tunnel are, on average, three times more lethal than accidents that occur on an open road (Bai, Liao, & Xia, 2020). Indeed, tunnel fires were the cause of catastrophic events worldwide, in which several people were injured or lost their lives, while tunnel facilities suffered extensive damage (Carvel & Marlair, 2005; Fridolf, Nilsson, & Frantzich, 2013; Leitner, 2001; Ren, Zhou, Hu, He, & Wang, 2019; Vuilleumier, Weatherill, & Crausaz, 2002).

Among the different tunnel safety aspects that can be taken into account to reduce the risk in case of fire, forced ventilation systems are one of the most essential. The importance of ventilation systems is twofold (European Commission, 2004): (i) the control of pollutants emitted by road vehicles under normal traffic flow, peak traffic flow and traffic jams; (ii) the control of heat and smoke in case of a fire. The typology of the ventilation system for fire control is typically dictated by the traffic mode (i.e. one- or bi-directional) and by the traffic flow regime (congested or uncongested).

With a one-directional road and uncongested traffic, longitudinal ventilation is the simplest and most cost-efficient solution (figure 1a). With this strategy, the toxic smoke is pushed downstream of the vehicles by a longitudinal flow that blows in the same direction as the travelling cars. The drivers upstream of the fire can then safely evacuate, as far as the longitudinal ventilation velocity is able to prevent the development of the back-layering flow, namely a horizontal gravity current generated at the tunnel ceiling that propagates also upstream of the fire source (Salizzoni et al., 2018; Vauquelin, 2008). The minimum air velocity required to keep the upwind portion of the tunnel entirely free of smoke is referred to as the ‘critical velocity’ (Danziger & Kennedy, 1982; Thomas, 1958, 1968). Its dependence on the main factors characterising the tunnel fire has been the subject of numerous studies over the years (e.g. Grant, Jagger, & Lea, 1998; Hu, Huo, & Chow, 2008; Ingason & Li, 2010; Jiang, Creyssels, Mos, & Salizzoni, 2018; Le Clanche et al., 2014; Li, Lei, & Ingason, 2010; Vauquelin & Wu, 2006). The main drawback of longitudinal ventilation systems is that they tend to destroy the fire-induced thermal stratification of the buoyant smoke whenever the velocity is excessively high, so that the downstream tunnel stretch ends up being entirely filled with smoke (Yang et al., 2010).

On the other hand, transverse ventilation systems (figure 1b) are appropriate for a bi-directional road and/or congested traffic. Transverse ventilation systems are generally composed of ventilation ducts located above a false ceiling, connected to the tunnel by remote-controlled dampers; alternatively, ventilation shafts fitted with fans may be used (Li & Chow, 2003). The smoke is therefore extracted by vents displaced on the tunnel ceiling. In optimal operating conditions, the smoke should be confined within the extraction zone delimited by two adjacent vents, enabling the evacuation of tunnel users in the two directions (i.e. both upstream and downstream of the fire source). At the same time, the flow should be kept stratified during the extraction, with the hot smoke lying in the upper part of the ceiling, therefore allowing uncontaminated ambient air to circulate in the lower part (figure 1b). Keeping stably stratified conditions is crucial to allow rescue and safety operations to be conducted, especially in the initial stages of a fire. Indeed, the longer the flow maintains its stratification, the longer it enables evacuation procedures. To preserve stratified smoke conditions, the longitudinal flow velocity induced by the action of the vertical vents should be as close as possible to zero near the fire. In order to keep the smoke layer confined within the extraction zone, establishing convergent flows towards this zone is required, but generally not sufficient. Indeed, if the smoke is not entirely removed from the tunnel

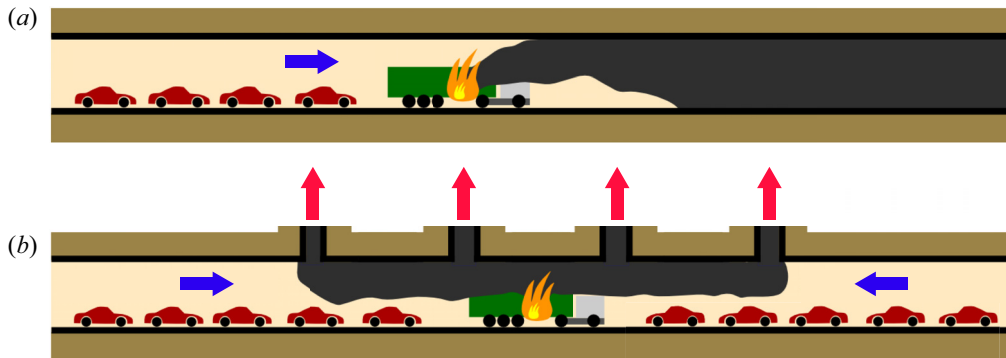


Figure 1. Example of (a) longitudinal ventilation system; (b) transverse ventilation system. The blue arrows indicate the longitudinal velocity while the red arrows represent the vertical extraction velocity. Source: modified from Kubwimana (2020).

through the dampers, its buoyancy will force it to propagate away from the duct location, forming a sort of back-layering flow. In general, transverse ventilation systems are more complex to manage compared with longitudinal ones since their optimal operating conditions depend on a larger number of factors (Chaabat et al., 2020; He et al., 2018; Lovas, Carlotti, Desanghère, & Mos, 2011; Oucherfi, Gay, Mos, & Carlotti, 2009; Tao & Zeng, 2022).

A recent systematic study on the aerodynamics of a transverse ventilation system was provided by Chaabat et al. (2020), who examined the ideal case of symmetrical ventilation on smoke propagation and determined the governing parameters for the confinement velocity, i.e. the vertical velocity that enables confining of the smoke to the extraction zone. This particular configuration requires an excellent regulation of the longitudinal air flow in the tunnel as a whole and, therefore, dedicated equipment (such as jet fans) controlled in real time using accurate velocity measurements made in unperturbed areas of the tunnel (e.g. Levoni, Angeli, Cingi, Barozzi, & Cipollone, 2021). In many real cases, this ideal flow control cannot be achieved for a number of reasons. For instance, short tunnels may not have a sufficiently long unperturbed zone (i.e. free of smoke and sufficiently far away from jet fans) to perform reliable velocity measurements. Older tunnels may also not have state-of-the-art equipment, nor available space to install it. Less-than-ideal air flow control results in a certain degree of asymmetry in the flow. This asymmetry may also be voluntary, as in the case of unidirectional tunnels in which the preferred direction of the smoke is the traffic direction or when mobile fan units are employed to generate a longitudinal flow to improve the effectiveness of the existing ventilation system in emergencies (Jiang & Ingason, 2020).

Another aspect to take into account in designing tunnel ventilation systems is the occurrence of natural ventilation currents, driven by the wind-induced pressure difference between the two tunnel portals (Kubwimana et al., 2018) or by large-scale meteorological effects, as in the case of synoptic pressure differences occurring on the opposite sides of alpine tunnels. Indeed, these can modify the ventilation operation systems by imposing an additional longitudinal flow (He et al., 2020).

For these reasons, there is a rising interest in studying transverse ventilation systems in asymmetric flow conditions, as dictated by natural ventilation, non-ideal operational conditions or by the necessity to implement both longitudinal and transverse systems (usually referred to as ‘combined ventilation systems’), since they may overcome some limitations of the two classical modes (Brousse, Voeltzel, Le Botlan, & Ruffin, 2002; Lee, Oh, Oh, Yoo, & Shin, 2010; Li & Chow, 2003).

Chen et al. (2015) investigated the effect of an increasing distance between the vent on the tunnel ceiling and the heat source, reporting that the larger the distance, the longer the extent of the back-layering length. Tang et al. (2017) studied the buoyant smoke stratification conditions that occur in a combined ventilation system while other authors (Tang, He, Mei, Wang, & Zhang, 2018; Tang, Li, Mei, & Dong, 2016; Yao et al., 2016) reported experiments in which different transverse extraction modes

were tested (shaft, vent and centralised mechanical ventilation). In addition, [Zhu, Tang, Chen, Wang, and Xu \(2020\)](#) analysed the effectiveness of a smoke extraction vent placed on tunnel sidewalls in terms of back-layering length and critical velocity. Besides these laboratory experiments, some analytical models were proposed to predict the back-layering length in the case of transverse ventilation systems subjected to a longitudinal flow, reporting a remarkable match with laboratory ([Tang et al., 2016](#); [Wang et al., 2018](#)) or field ([Cingi et al., 2021](#); [Levoni et al., 2015](#)) data.

Despite the increasing attention to this topic, there are several aspects that still need to be clarified. To push further our understanding of the flow dynamics in tunnels in the presence of both a transverse and longitudinal forcing, we report herein the results of a series of experiments performed within a reduced-scale tunnel. The experimental set-up is the same as the one recently used by [Chaabat et al. \(2020\)](#). The flow in the tunnel is induced by the presence of a buoyant release, simulating a fire ([Vauquelin, 2008](#); [Vauquelin, Michaux, & Lucchesi, 2009](#)), and by the mechanical forcing due to (i) extraction vents at the ceiling and (ii) a longitudinal flow imposed by a longitudinal pressure gradient. In this framework, we have analysed the confinement conditions of the buoyant release in terms of (i) the extraction mean velocity, (ii) the flow rate and (iii) the stratification conditions of the flow. Each of these aspects has been studied by adopting different rectangular-shaped vents, variably positioned (centrally or laterally), as well as using vertical solid barriers placed at the tunnel ceiling. Notably, the application of barriers has proved to be very effective in reducing smoke spreading, both with longitudinal ([Chaabat et al., 2019](#); [Seike, Kawabata, & Hasegawa, 2014](#)) and transverse ([Chaabat et al., 2020](#); [Halawa & Safwat, 2021](#)) ventilation systems. Their effectiveness was, however, never tested in combined ventilation systems. From a practical point of view, with this work we try to answer the following questions:

- For a given imbalance of the longitudinal air flow, what increase in the extraction flow rate (compared with the symmetrical situation) is required to keep the smoke confined within the extraction zone?
- Are given damper shapes still significantly more effective than others when the flow is unbalanced?
- To which extent is smoke stratification in the extraction zone affected by the asymmetry of the flow?

This work is structured as follows: in § 2 we identify the parameters governing the flow dynamics through a dimensional analysis, while § 3 describes the tunnel facility used during the experimental campaign (§ 3.1) and summarises the conditions set in each test (§ 3.2). Section 4 presents and discusses the experimental results in terms of the confinement conditions (§ 4.1) and flow regime (§ 4.2). Conclusions are drawn in § 5.

2. Dimensional analysis and similarity conditions

In analogy with what was presented in previous studies ([Chaabat et al., 2020](#); [Le Clanche et al., 2014](#); [Salizzoni et al., 2018](#)), we perform a dimensional analysis to identify the governing parameters of the flow dynamics. To this end, we consider a flow in an infinitely long tunnel with a fixed rectangular cross-section and equipped with both a longitudinal and transverse ventilation system. A circular source, located along the longitudinal axis of the tunnel floor, releases steadily a buoyant fluid of variable density. In this context, our focus is on the conditions that allow for the confinement of the buoyant release within two extraction fans, therefore preventing the possible formation of a back-layering flow at the tunnel ceiling, whose extent is referred to as L in [figure 2\(a\)](#). Thus, by definition, a confinement condition is characterised by a null value of the back-layering length L . The extraction velocity which realises such a ‘confinement’ is here referred to as $U_{e,c}$, and defined as the minimum value of the ratio between the flow extracted by the vents that guarantees $L = 0$ and the cross-sectional area of the vents.

The ‘confinement’ velocity $U_{e,c}$ depends on the following parameters: the tunnel geometry (i.e. tunnel height H and width W), the characteristics of the buoyant release at the source (its density ρ_s , its velocity W_s and the diameter of the source D_s), the longitudinal velocity (referred to as U_l and defined as the flow rate of fresh air entering the tunnel divided by the cross-sectional area of the tunnel), the characteristics of the rectangular-shaped vertical vents (the length of the two sides, i.e. l_x and l_z , and the spanwise distance between the damper centre and the tunnel centreline z_c , see [figure 2\(d\)](#)), the physical properties

of the ambient fluid (the density ρ_0 , the kinematic viscosity ν and the molecular diffusivity D_m) and the gravitational acceleration g . For the sake of simplicity, we neglect possible differences between the viscosities and molecular diffusivities of the two fluids (i.e. the ambient air and the buoyant release). We can therefore formulate the following functional dependence:

$$U_{e,c} = f(W_s, U_t, \rho_s, \rho_0, \nu, D_m, H, W, D_s, l_x, l_z, z_c, g), \quad (2.1)$$

involving thirteen dimensional quantities with three independent dimensions (time, length and mass). By invoking the Vaschy–Buckingham theorem (Barenblatt, 1996), we can therefore express (2.1) in a non-dimensional form, displaying the dependence of a normalised confinement velocity $U_{e,c}/U_t$ by means of ten non-dimensional controlling parameters

$$\frac{U_{e,c}}{U_t} = f\left(\Gamma_s, Re_s, Sc, \frac{\rho_s}{\rho_0}, \frac{W_s}{U_t}, \frac{D_s}{H}, \frac{W}{H}, \frac{A_d}{H^2}, S_d, P_d\right), \quad (2.2)$$

where $Re_s = W_s D_s / \nu$ is the source Reynolds number, $Sc = D_m / \nu$ is the Schmidt number, $A_d = l_x l_z$ is the damper opening area, $S_d = l_x / l_z$ is the damper aspect ratio, $P_d = z_c / H$ is the spanwise damper position, and Γ_s is the plume Richardson number at the source, defined as

$$\Gamma_s = \frac{5}{16\alpha} \frac{g(\rho_0 - \rho_s)}{\rho_0} \frac{D_s}{W_s^2} = \frac{5}{4\pi\alpha} \frac{B_s}{W_s^3 D_s}, \quad (2.3)$$

where $\alpha = 0.127$ is a reference value for the top-hat entrainment coefficient for a pure plume (Ezzamel, Salizzoni, & Hunt, 2015; Hunt & Kaye, 2005; Morton, Taylor, & Turner, 1956) and $B_s = W_s A_s g(\rho_0 - \rho_s) / \rho_0$ is the buoyancy flux at the source, with $A_s = \pi D_s^2 / 4$ the area of the source. As is well known (Hunt & Kaye, 2005), the plume Richardson number allows for a classification of the buoyant releases. Notably, $\Gamma_s = 1$ indicates a pure plume, i.e. having a dynamical equilibrium between momentum and buoyancy flux; $\Gamma_s < 1$ indicates a forced plume (Morton, 1959), characterised by an excess of momentum compared with the buoyancy flux; and $\Gamma_s > 1$ indicates a lazy plume (Hunt & Kaye, 2005), in which the buoyancy flux exceeds the momentum flux. This latter category includes most plumes from solid or liquid fires (Heskestad, 1998). Considering a constant Schmidt number, a constant diameter of the source D_s , a fixed tunnel geometry (i.e. a constant aspect ratio W/H) and a constant damper opening area A_d , (2.2) reduces to

$$\frac{U_{e,c}}{U_t} = f\left(\Gamma_s, Re_s, \frac{\rho_s}{\rho_0}, \frac{W_s}{U_t}, S_d, P_d\right). \quad (2.4)$$

As illustrated by the previous works of Jiang et al. (2018) and Jiang, Creyssels, Hunt, and Salizzoni (2019), the functional dependence expressed by (2.4) can be further simplified. Firstly, we can assume that the flow becomes independent on the Reynolds number when this exceeds a given critical value (typically $Re_c = 600$, according to Arya & Lape, 1990). Secondly, in the case of buoyancy-dominated releases ($\Gamma_s > 1$), as shown by Jiang et al. (2019) and Chaabat et al. (2020), the influence of both Γ_s and ρ_s / ρ_0 fades out. Indeed, buoyancy-dominated releases lose information about the source conditions, presumably due to the enhanced mixing in the near-source region that characterises lazy plumes (Jiang et al., 2019; Marjanovic, Taub, & Balachandar, 2017). In these conditions, we expect the confinement velocity $U_{e,c}$ to lose dependence on the individual source parameters, i.e. ρ_s , W_s and D_s , which would play instead a role only by imposing a buoyancy flux B_s . The formulation of the problem can therefore be simplified considerably as

$$U_{e,c} = f(B_s, U_t, H, S_d, P_d), \quad (2.5)$$

or, in non-dimensional form, as

$$Fr_{e,c} = f(Fr_t, S_d, P_d), \quad (2.6)$$

where

$$Fr_t = \frac{U_t}{(B_s/H)^{1/3}}, \quad (2.7)$$

$$Fr_{e,c} = \frac{U_{e,c}}{(B_s/H)^{1/3}} \quad (2.8)$$

are the ‘tunnel’ and the ‘extraction’ Froude numbers, respectively, quantifying the ratio between inertia forces (induced by the longitudinal or transverse ventilation system) and the buoyancy forces (induced by the source). Of course, other functional dependencies could be retrieved by adopting different non-dimensional governing parameters. Notably, several authors characterise the flow dynamics by means of the tunnel Richardson number which, in our case, would be simply defined as $Ri = Fr^{-1/3}$ (Salizzoni et al., 2018). Equivalently, we can also consider a modified Froude number, integrating information about the damper opening area A_d and the tunnel cross-sectional area $\Omega = WH$, and defined as

$$Fr_{e,c}^* = \frac{A_d}{\Omega} \frac{U_{e,c}}{(B_s/H)^{1/3}} = \frac{A_d}{H^2} \frac{W}{H} Fr_{e,c}. \quad (2.9)$$

In this modified Froude number, obtained by combining three non-dimensional parameters (see (2.2)), the influence of A_d is *de facto* removed (since $A_d U_{e,c} = Q_{e,c}$), thus implying that the relevant velocity scale would be the one which characterises the impact of the extraction flow on the buoyant release within the tunnel, rather than the extraction velocity at the vents (which of course highly depends on the geometry of the vents themselves). However, since A_d and Ω are fixed in the present study, the two Froude numbers only differ by a proportionality constant. Based on our results we, therefore, cannot evaluate which of the two is more appropriate to re-scale the flow variables.

Equation (2.6) defines the similarity conditions for the tunnel ventilation in the presence of a steady source of buoyancy released at the tunnel floor, assuming a fully turbulent flow. To make a link between this idealised condition and a real tunnel fire, we first need to establish a link between the power emitted during the combustion and the actual buoyancy flow released by a fire. The latter is computed as $B_s = g\dot{Q}_s/\rho_0 T_0 C_p$ (Linden, 2000), where \dot{Q}_s is the fire heat release rate (HRR), T_0 is the reference ambient air temperature and C_p its specific heat capacity at constant pressure. Note that part of the HRR is actually transferred as a radiative flux, heating the surrounding walls, that in turn heat back the ambient air and the smoke mixture. In engineering practice, these complex heat exchange mechanisms are usually neglected when providing a first estimate of the ventilation conditions. It then simply considered that a fraction of the HRR is ‘lost’ in radiation, therefore not contributing to the convective flux, hence to the buoyancy flux. According to the PIARC Committee on Road Tunnels (1999) report, this fraction lies in a range between 20 % and 50 % of the HRR. More specifically Drysdale (2011), in the general context of fire dynamics, suggests a value of 30 %, which agrees well with the estimates presented by Carlotti, Vallerent, Fromy, and Demouge (2012), based on systematic comparisons between models and experiments. Considering an ambient air at 20 °C (i.e. $\rho_0 = 1.204 \text{ kg m}^{-3}$, $T_0 = 293.15 \text{ K}$ and $C_p = 1.006 \text{ kJ (kg K)}^{-1}$), a tunnel height $H = 5 \text{ m}$ and estimated HRRs representative of a burning vehicle (10 MW), van (30 MW) and heavy goods truck (100 MW), we can therefore compute the typical values of Fr_t for varying air flow velocities U_t (see table 1). The question is to identify the range of the Froude numbers for which the buoyant smokes are confined within two dampers. Besides, it is essential to know if the confinement conditions guarantee a stable stratification of the buoyant smokes, depending on the shape of the vents. The object of this study is therefore to determine the functional dependence expressed by (2.6) and enlighten the associated flow regimes, depending on the flow stratification. For that purpose, we have planned an experimental campaign to unveil the dependence on the non-dimensional confinement velocity and the different governing parameters.

Finally, it is worth remembering that the similarity conditions expressed by (2.6) can be used to estimate ventilation velocities in real tunnel fires only as far as the fire flames have a limited extension in the vertical direction, so that they can be reliably represented by a steady source of buoyancy placed at

Table 1. Values of Fr_t for usual values of fire heat release rates \dot{Q}_s and corresponding longitudinal air flow velocity in transverse ventilation systems. Note that \dot{Q}_s was reduced by 30 % to account for lost heat.

		\dot{Q}_s		
		10 MW	30 MW	100 MW
U_t	1 m s ⁻¹	0.30	0.21	0.14
	2 m s ⁻¹	0.59	0.41	0.27
	3 m s ⁻¹	0.89	0.62	0.41
	4 m s ⁻¹	1.18	0.82	0.55

the tunnel floor. As verified by Jiang et al. (2018) using numerical simulations, this condition holds until the flames do not exceed the tunnel half-height. Of course, applications to real fires would also require consideration of the presence of vehicles and their blocking effect on the ventilation flow (Chaabat et al., 2019).

3. Experimental methodology

3.1. Facility set-up and measurement techniques

The experimental campaign was conducted in a 1/25 reduced-scale tunnel facility (figure 2a) installed at the Fluid Mechanics and Acoustics Laboratory (LMFA) of the École Centrale de Lyon, France. The scaled tunnel is 8.4 m long, with a rectangular cross-section that is 0.36 m wide and 0.18 m high. To allow the flow to be visualised, one sidewall is made of tempered glass while the other sidewall, the floor and the ceiling are made of black medium-density fibreboard panels. The longitudinal flow (figure 2a) is induced by the combined effect of the two fans placed on the tunnel ceiling and the extraction fan placed at the left end of the tunnel. For this latter, we could control the working point of the fan (in terms of revolutions per minute). In the absence of extraction fans on the tunnel ceiling, this would have produced an outflow rate Q_{out} between 20 and 355 m³ h⁻¹. However, as verified *a posteriori* (i.e. once the experiments were run), imposing a ‘confinement condition’ implied a Q_{out} always directed towards the interior of the tunnel, despite the action of the fan placed at the tunnel end. The inlet flow rate Q_{in} is measured by means of an air flow cone equipped with a Pitot tube (precision 1 Pa) located at the tunnel entrance (figure 2a). The related longitudinal mean velocity is easily estimated as $U_t = Q_{in}/\Omega$, where Ω is the area of the tunnel cross-section (equal to $2H^2$ since the tunnel width W is two times the tunnel height H).

Fire-induced smoke is simulated by releasing a light gas (a mixture of air and helium) into the tunnel, an approach widely adopted in the literature (Alva, Jomaas, & Dederichs, 2017; Chaabat et al., 2019, 2020; Jiang et al., 2019; Le Clanche et al., 2014; Vauquelin, 2008). To visualise the buoyant release, oil droplets are used to seed the air–helium mixture, so that it becomes clearly visible in the ambient air when illuminated with a green laser plane.

The light gas is released from a circular source (diameter $D_s = 0.1$ m) placed on the longitudinal centreline of the tunnel floor. The released air–helium mixture and its seeding are controlled by means of three flow meters (Alicat Scientific Inc., MC-Series, USA). This type of flow meter has an error on the flow rate that does not exceed ± 3 % if compared with classical volumetric counters (Nironi et al., 2015; Vidali et al., 2022). The air and helium flow rates can be varied up to 500 l min⁻¹ (precision 2.5 l min⁻¹) and 200 l min⁻¹ (precision 1 l min⁻¹), respectively, while the flow rate of the air with nebulised oil can reach a maximum discharge of 20 l min⁻¹ (precision 0.1 l min⁻¹).

On the tunnel ceiling, two extraction vents are located symmetrically from the source centre and spaced by $5H$ (figure 2a). On each side, the extraction air flow rate is guaranteed by the presence of a centrifugal fan (flow rate spanning between 5 and 150 m³ h⁻¹) and measured by means of a rotameter

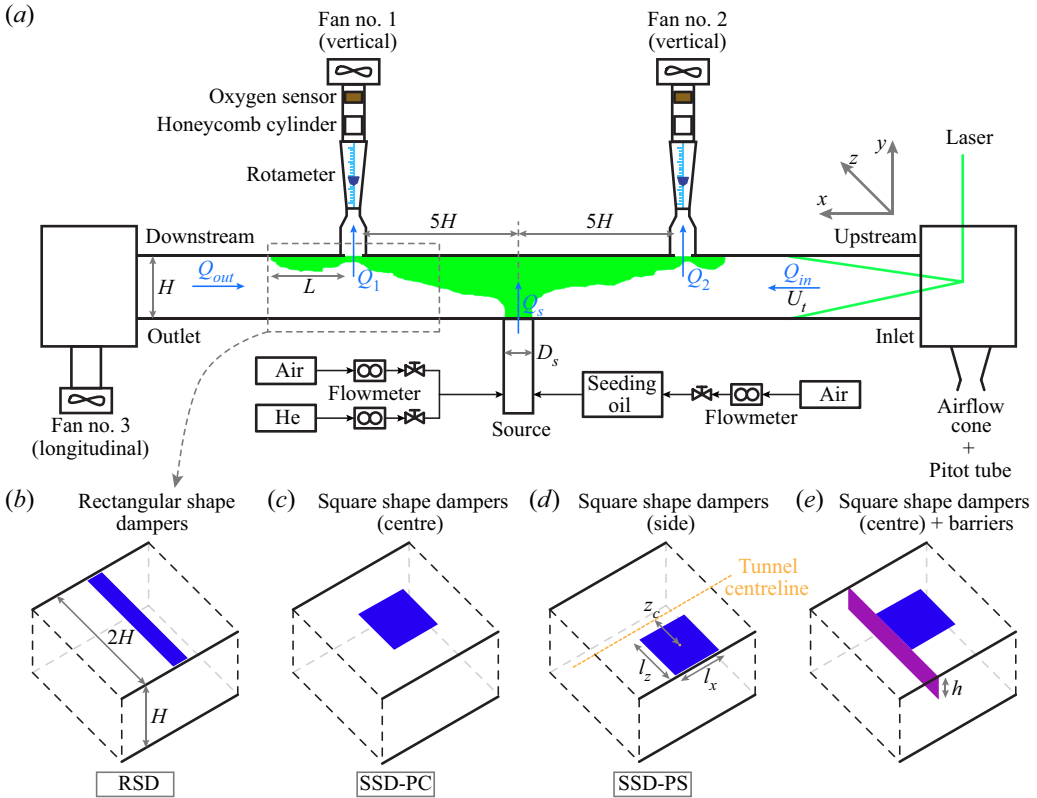


Figure 2. (a) Overview of the tunnel facility used for the experiments together with the instrumentation. The detail of the flow pattern within the tunnel is schematised by light blue arrows. Panels (b–d) report the shape and disposition of the different dampers displaced in the tunnel ceiling: (b) dampers with a transverse rectangular shape (RSD); (c) dampers with a square shape placed on the tunnel ceiling centre (SSD-PC); (d) dampers with a square shape placed on the tunnel ceiling side (SSD-PS). In addition, panel (e) shows the experimental set-up with the large barriers adopted ($h = H/3$). Panel (e) displays only the case SSD-PC with the barriers, but the same disposition is applied to the other types of dampers.

(precision 1 l s^{-1}) placed in the extraction duct (see Chaabat et al., 2020). Part of the tunnel ceiling hosting the vents is easily adjustable so that the vent shape and the duct extension can be modified. Note that the linear scale of the rotameter is designed considering air as working fluid. Since we are instead dealing with a mixture of air and helium, we have to apply a correction of the flow rate estimate, depending on the actual flow density. For this, a sensor (Winsen, Grove - Gas Sensor, Singapore) measuring the oxygen concentration (precision 2%) in the air flow extracted by the vents is positioned above each rotameter. This, in turn, provides the helium concentration and hence the fluid density. A honeycomb cylinder is mounted to protect the oxygen sensor from the oil drops that could hamper its functionality. The procedure used to link the flow rate provided by the rotameter (Q_{r1} or Q_{r2}) with the actual value of the mixture flow rate (Q_1 or Q_2) was defined by Chaabat et al. (2020) for the same rotameter used herein (i.e. the one with a nominal measurement range spanning between 16 and $160 \text{ m}^3 \text{ h}^{-1}$). Briefly, by varying the density ratio ρ_s/ρ_0 and the flow rate in the entrance to the rotameter, we obtain linear relationships of the form $Q_1 = \beta_1(\rho_s/\rho_0)Q_{r1}$ and $Q_2 = \beta_2(\rho_s/\rho_0)Q_{r2}$, where the constants β_1 and β_2 depend on the ratio ρ_s/ρ_0 and instrument factory features.

Figure 2(a) also shows the general flow pattern inside the tunnel during the experiments (light blue arrows). In each experiment, the flow rates Q_1 and Q_2 at the vents are known, together with the

corresponding densities (ρ_1 and ρ_2), because they are measured by the rotameters and oxygen sensors, respectively. Furthermore, also Q_s and ρ_s at the source are known, since they are set by the users as boundary conditions of the problem. At the tunnel inlet, the flow density is ρ_0 and the flow rate Q_{in} is directly obtained by means of the Pitot tube in the air flow cone (figure 2a). The outflow Q_{out} can then be determined by invoking mass conservation

$$Q_{out} = \frac{1}{\rho_{out}}(\rho_0 Q_{in} + \rho_s Q_s - \rho_1 Q_1 - \rho_2 Q_2). \quad (3.1)$$

Since we are also assuming that all the light fluid is extracted at the ceiling, i.e. $\rho_{out} = \rho_0$, we have

$$Q_{out} = Q_{in} + \frac{1}{\rho_0}(\rho_s Q_s - \rho_1 Q_1 - \rho_2 Q_2). \quad (3.2)$$

Note that, despite the action of the vent placed at the end of the tunnel, the actual direction of the flow rate Q_{out} is always negative (as shown in figure 2(a) and § 4.1.1). This is due to the flow conditions produced by the fans at the ceiling inducing a current in the two tunnel stretches placed upstream and downstream of the two vents and directed towards them, to which we refer as a ‘suction effect’.

Three different vent (or damper) shapes were employed during the experiments, all having the same opening area $A_d = 0.011 \text{ m}^2$ (figure 2b–d). We used the same dampers adopted by Chaabat et al. (2020), notably:

- A damper with a transverse rectangular shape ($0.32 \times 0.034 \text{ m}$) which occupies almost the entire width of the tunnel, hereinafter called RSD (figure 2b).
- A damper with a square shape ($0.104 \times 0.104 \text{ m}$) centred with respect to the tunnel centreline, hereinafter called SSD-PC (figure 2c).
- A damper with a square shape ($0.104 \times 0.104 \text{ m}$) positioned on a side with respect to the tunnel centreline, hereinafter called SSD-PS (figure 2d).

Note that side-positioned square-shape dampers (SSD-PS) are the most common configuration in actual tunnels (e.g. the Trans-Alpine Fréjus Road Tunnel connecting France and Italy), since a fresh air duct is often present next to the smoke extraction duct.

Additionally, we tested the effect of vertical barriers in order to enhance the vents’ capture efficiency (figure 2e). Two planar barriers were hung on the tunnel ceiling close to the vents’ extremity. The height and width of the barriers were $h = H/3$ and $2H$ (i.e. equal to the tunnel width), respectively, and were sufficiently rigid to withstand the aerodynamic forces induced by the flow.

3.2. Experimental procedure

Thanks to the great versatility of the facility, the flow within the tunnel could be modified by varying the following control parameters: (i) the density of the buoyant release; (ii) the velocity at the source of the buoyant release; (iii) the longitudinal mean velocity in the tunnel; (iv) the vertical mean extraction velocity of the vents; (v) the shape of the vents; and (vi) the presence of the barriers. Once the confinement condition is attained, the flow exhibits different stratification behaviours, depending on the setting of the control parameters (we will discuss this point in more detail in § 4.2).

A total of thirteen tests were conducted (table 2) and each of them included 7 to 14 measurements (except for test 12, which has only one measure). For each test, we estimated the mean extraction velocity guaranteeing confinement conditions, depending on a varying intensity of the longitudinal velocity U_t , varying source conditions and/or vents configurations (vent shape and position as well as the presence of barriers). In most of the tests, we also analysed the stratification conditions within the tunnel.

Each test started by turning on all three fans at the minimum regime. Once the longitudinal velocity at the tunnel inlet became stable, the flowmeters controlling the buoyant release were also turned on. At this stage, the extraction velocity was weak, so that the released buoyant fluid could spread within the whole

Table 2. Summary of experiments and associated fluid dynamic conditions. The columns indicate: the source Reynolds number Re_s , where the kinematic viscosity of the gas mixture was calculated using the approach proposed by Herring and Zipperer (1936); the plume Richardson number Γ_s ; the density ratios ρ_s/ρ_0 and ρ_e/ρ_0 , where $\rho_e = (\rho_1 + \rho_2)/2$ is the density of the extracted air–helium mixture; the tunnel Froude number Fr_t ; the extraction Froude number in the confinement condition $Fr_{e,c}$; the modified extraction Froude number $Fr_{e,c}^*$; the longitudinal mean velocity within the tunnel U_t ; and the equivalent fire HRR \dot{Q}_s , already reduced by 30%. The last three columns report the shape of the vents, the presence of the barriers and the evaluation or not of the stratification conditions, respectively.

Run	Re_s (-)	Γ_s (-)	ρ_s/ρ_0 (-)	ρ_e/ρ_0 (-)	Fr_t (-)	$Fr_{e,c}$ (-)	$Fr_{e,c}^*$ (-)	U_t (m s ⁻¹)	\dot{Q}_s (kW)	Vent		Stratification evaluation
										Shape	Barriers	
Test 1	3040	1.6	0.74	0.88–0.94	0.35–2.39	2.09–9.92	0.36–1.68	0.15–1.01	0.32	RSD	X	X
Test 2	2280	3.0	0.74	0.91–0.95	0.46–2.78	2.31–10.26	0.39–1.74	0.18–1.05	0.23	RSD	X	X
Test 3	2890	1.9	0.72	0.91–0.94	0.60–2.10	3.60–8.91	0.61–1.51	0.25–0.88	0.33	RSD	X	X
Test 4	2100	3.7	0.72	0.85–0.92	0.25–2.49	1.95–9.64	0.33–1.64	0.10–0.94	0.24	RSD	X	✓
Test 5	1480	7.4	0.72	0.84–0.95	0.31–3.16	2.01–11.77	0.34–2.00	0.07–1.06	0.17	RSD	X	✓
Test 6	1800	3.7	0.45	0.80–0.89	0.35–1.36	2.35–6.09	0.40–1.03	0.19–0.70	0.65	RSD	X	✓
Test 7	1050	14.8	0.72	0.87–0.94	0.27–3.32	2.13–12.18	0.36–2.07	0.08–0.99	0.12	RSD	X	✓
Test 8	1210	3.7	0.26	0.74–0.89	0.32–1.57	2.31–6.55	0.39–1.11	0.20–0.96	1.03	RSD	X	✓
Test 9	2080	3.7	0.72	0.88–0.94	0.32–2.52	2.60–10.73	0.44–1.82	0.12–0.95	0.24	RSD	✓	✓
Test 10	2120	3.7	0.72	0.91–0.92	1.33–2.57	7.12–11.32	1.21–1.92	0.50–0.98	0.24	SSD-PC	X	✓
Test 11	2120	3.7	0.72	0.89–0.93	0.49–2.93	3.31–10.88	0.56–1.85	0.18–1.10	0.24	SSD-PC	✓	✓
Test 12	2120	3.7	0.72	0.93	2.27	11.28	1.91	0.85	0.24	SSD-PS	X	✓
Test 13	2110	3.7	0.72	0.91–0.92	1.26–2.73	6.76–11.20	1.18–1.90	0.47–1.03	0.24	SSD-PS	✓	✓

tunnel. The extraction velocity of the vertical fans was then progressively increased, always imposing the same flow extracted by both fans. When the confinement condition was attained, i.e. with the buoyant release bounded between the two vents, we registered the value of the two extraction velocities, as well as the value of U_t . The extraction velocity in confinement conditions $U_{e,c}$ was then computed as the average between the values registered at fan no. 1 and fan no. 2 (figure 2a), i.e. $U_{e,c} = (U_{e,c1} + U_{e,c2})/2$, where $U_{e,c1} = Q_1/A_d$ and $U_{e,c2} = Q_2/A_d$. Considering all the experiments, the difference between the extraction velocities at the two vents was approximately 10 % at most and systematically higher in fan no. 1, presumably due to the inherent asymmetry of the system. To further explore the relationship between U_t and $U_{e,c}$, the longitudinal velocity was slightly increased and the above procedure was repeated. A test was stopped when the flow rate at the extraction vents exceeded the rotameter measurement range.

The values of the governing parameters for each experimental test are listed in table 2. All the experiments were performed with a $\Gamma_s > 1$, i.e. with buoyancy-dominated releases, in the range $1.6 \leq \Gamma_s \leq 14.8$ with a density ratio of $0.26 \leq \rho_s/\rho_0 \leq 0.74$. The values of the Reynolds number at the source are in the range $1050 \leq Re_s \leq 3040$, i.e. well above the critical value $Re_c = 600$ indicated by Arya and Lape (1990). The values of $Fr_{e,c}$ were always higher than 1 in all tests, while Fr_t had values both lower and higher than 1 in all the experiments involving the rectangular-shaped dampers (RSD).

4. Results and discussions

In the following, we report the results obtained in the experimental campaign. All data are displayed together with the associated measurement uncertainty, estimated as a type B uncertainty (Joint Committee for Guides in Metrology, 2008) considering the manufacturer's specifications for each instrument and expressed in the form of an error bar. Whenever the data are shown without an error bar, this means that the associated uncertainty is lower than the marker size used in the plots.

4.1. Confinement conditions

4.1.1. Velocity

As a first step, focusing on the RSD, we have used our experimental data to unveil the functional dependence between Fr_t and $Fr_{e,c}$ and expressed in (2.6). As shown in figure 3(a,b), all the data collapse fairly well on a curve of the form

$$Fr_{e,c} = aFr_t + b \quad (\text{or } Fr_{e,c}^* = a^*Fr_t + b^*), \quad (4.1)$$

in which the value of the two coefficients $a = 3.45$ and $b = 1.13$ (or $a^* = 0.59$ and $b^* = 0.19$) were determined by means of a best linear least-square fitting of the data ($R^2 = 0.99$ and $RMSE = 0.30$). According to (4.1), it is evident that, for a fixed B_s , as the longitudinal velocity increases, a higher extraction velocity is necessary to confine the buoyant flow, and *vice versa*. Beside setting experimentally the relation established by (2.6), we also aim at certifying the reliability of the assumptions that led to its formulation. We stress that this functional dependence is based on the assumption that the flow dynamics is not sensitive to the source parameters Γ_s and ρ_s/ρ_0 , a condition that is expected to hold only for $\Gamma_s > 1$ (i.e. buoyancy-dominated releases). To verify this, we have performed experiments imposing varying values of Γ_s and ρ_s/ρ_0 . The results shown in figure 3(a,b) clearly demonstrate that, as already verified by Jiang et al. (2019) for a pure longitudinal ventilation and Chaabat et al. (2020) for pure transverse ventilation, in the range of values herein considered ($\Gamma_s \in [1.6, 14.8]$ and $\rho_s/\rho_0 \in [0.26, 0.74]$), the flow dynamics is insensitive of varying values of both Γ_s (figure 3a) and ρ_s/ρ_0 (figure 3b). It is also worth noting that both series of experiments, at constant ρ_s/ρ_0 and constant Γ_s , imply a variability in the source Reynolds number of the buoyant releases. However, this variability has no relevant effect on the dependence of $Fr_{e,c}$ on Fr_t , therefore demonstrating that the flow is independent of Re_s , since it has attained a fully turbulent regime.

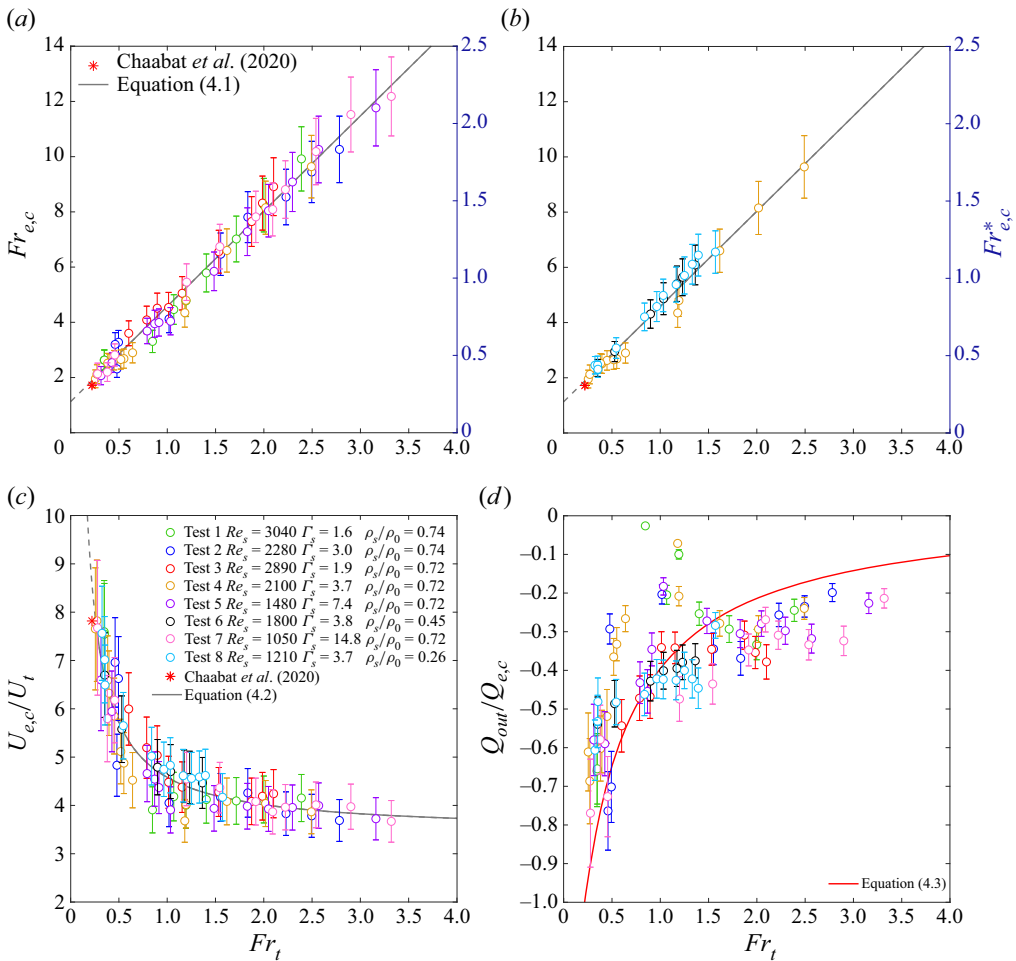


Figure 3. Panels (a–b) show the relationship between the tunnel Froude number Fr_t and the extraction Froude number $Fr_{e,c}$ in confinement conditions considering (a) a nearly constant density ratio ρ_s/ρ_0 (tests 1–5 and test 7) and (b) a constant plume Richardson number Γ_s (test 4, test 6 and test 8). The grey curves indicate the line of the best fit expressed by (4.1). Panel (c) reports the ratio between velocities $U_{e,c}/U_t$ as a function of the tunnel Froude number Fr_t . The grey line indicates (4.2). Finally, panel (d) reports the normalised outlet flow rate $Q_{out}/Q_{e,c}$ against the tunnel Froude number Fr_t together with the analytical curve expressed by (4.3). In panels (a–c), the datum of Chaabat et al. (2020) is drawn for comparison.

These results, combined with table 1, allow for the estimate of the confinement ventilation conditions within real tunnels. Considering a burning van, the confinement of the smoke would therefore require imposing velocities within the tunnel of approximately $U_t \simeq 2 \text{ m s}^{-1}$. Interestingly, even though not fully based on a scientifically grounded analysis, this is typically a reference value of the ventilation velocity imposed in a tunnel for engineering practice, when designing a ventilation system.

To highlight the relative role of the two competing velocities $U_{e,c}$ and U_t in confinement conditions, (4.1) can be rearranged as (figure 3c)

$$\frac{U_{e,c}}{U_t} = a + bFr_t^{-1}, \tag{4.2}$$

that shows how the dependence of the velocity ratio $U_{e,c}/U_t$ on the tunnel Froude number Fr_t progressively fades out as Fr_t increases. This implies that the presence of a source of buoyancy within the tunnel has a marginal role in the flow dynamics as $Fr_t \gtrsim 2$, so that the extraction velocity $U_{e,c}$ is almost fully determined by the forcing imposed by the longitudinal velocity U_t . This means that, as $Fr_t \gtrsim 2$, the buoyancy related to the light gas release progressively behaves as a passive scalar.

In figure 3(a–c) we also report the reference values ($Fr_t = 0.22$, $Fr_{e,c} = 1.72$ and $U_{e,c}/U_t = 7.82$) provided by Chaabat et al. (2020), for a transverse ventilation system without any imposed longitudinal flow. Note that the latter value represents the lower edge condition beyond which (4.1) and (4.2) cannot be extended. For this reason, in figure 3(a–c), this part of the fitted curves is drawn as a dashed line.

Once the vertical vents are activated, the downwind side of the tunnel undergoes a ‘suction effect’. In order to quantify its intensity, the flow rate in the tunnel stretch downstream of the vents was estimated through (3.2) (§ 3.1). As shown by the results reported in figure 3(d), we have that $Q_{out} < 0$, meaning that the air flow is directed towards the centre of the tunnel (figure 2a). For low Fr_t , when the longitudinal flow is small, the flow in the tunnel is governed by the extraction at the ceiling, so that $Q_{out}/Q_{e,c} \approx -1$ (where $Q_{e,c} = A_d U_{e,c}$). As the intensity of the longitudinal flow increases, the absolute value of the ratio $Q_{out}/Q_{e,c}$ progressively decreases and varies little as $Fr_t \gtrsim 2$. To express the evolution of $Q_{out}/Q_{e,c}$ for increasing Fr_t , we can deduce an analytical expression combining (3.2) and (4.1), which leads to

$$\frac{Q_{out}}{Q_{e,c}} = \frac{2H^2}{aA_d} \left(1 - \frac{b}{aFr_t + b} \right) - 2\frac{\rho_e}{\rho_0} + \frac{\rho_s}{\rho_0} \frac{Q_s}{Q_{e,c}}. \quad (4.3)$$

Note that (4.3) does not express a one-to-one dependence between $Q_{out}/Q_{e,c}$ and Fr_t , since its right-hand side explicitly depends also on other parameters such as ρ_e/ρ_0 and ρ_s/ρ_0 (which are not uniquely determined by the value of Fr_t). Notably, the ratio ρ_e/ρ_0 , that cannot be determined *a priori*, was observed to span the range 0.74–0.95, a variability that is likely to be due to the occurrence of plug holing (Liu & Yang, 2022) for high values of $Q_{e,c}$. This explains the larger scatter of the data in figure 3(d) (compared with that observed in figure 3(a–c)). Plotting (4.3) on the same graph requires setting the values of ρ_e/ρ_0 , ρ_s/ρ_0 and $Q_s/Q_{e,c}$. Adopting their respective averages, as determined over the experimental dataset for the tests 1–8, the trend in the data is reasonably well captured by (4.3).

4.1.2. The effects induced by using different vent shapes and barriers

So far we have focused on experiments with a fixed vent shape and varying source parameters (tests 1–8, table 2). As a further step, we consider the dependence of Fr_t on the vent shape and position ((2.6), figure 2b–d), keeping the source parameters unaltered. Furthermore, we also analyse the effects induced by large barriers placed close to the dampers’ end (figure 2e).

From an aerodynamic point of view, figure 4(a,b) indicates a departure from (4.1) and (4.2) when a different shape of the vent is employed. For instance, if we consider a fixed value of Fr_t , by switching from a rectangular shape to a square shape of the vents, we require a higher value of the extraction Froude number $Fr_{e,c}$ to attain confinement conditions (figure 4a), and *vice versa*. Furthermore, also a change in the position of the vents impacts negatively on the ventilation conditions needed to confine the buoyant release, since an even higher $Fr_{e,c}$ is required.

Therefore, we can state that the shape and position of the dampers significantly impact the conditions required to confine the buoyant smoke. As already exposed by Chaabat et al. (2020), the RSD leads to the best performance, while the SSD-PS is able to confine the buoyant plume only with very high velocities. This result is also in agreement with the findings by Oucherfi et al. (2009), based on numerical simulations, indicating that rectangular (slit) dampers show enhanced performance in terms of efficiency and yield with respect to dampers with different aspect ratio.

By assuming that the coefficient a is fixed in (4.1), new values for the coefficient b for the cases with squared vents can be found. In particular, we obtain $b = 2.42$ ($b^* = 0.40$) for the SSD-PC case and $b = 3.41$ ($b^* = 0.57$) for the SSD-PS case. These fitting curves (figure 4a,b) are also in agreement with the results of Chaabat et al. (2020) for the same vent shape (even though they are obtained adopting

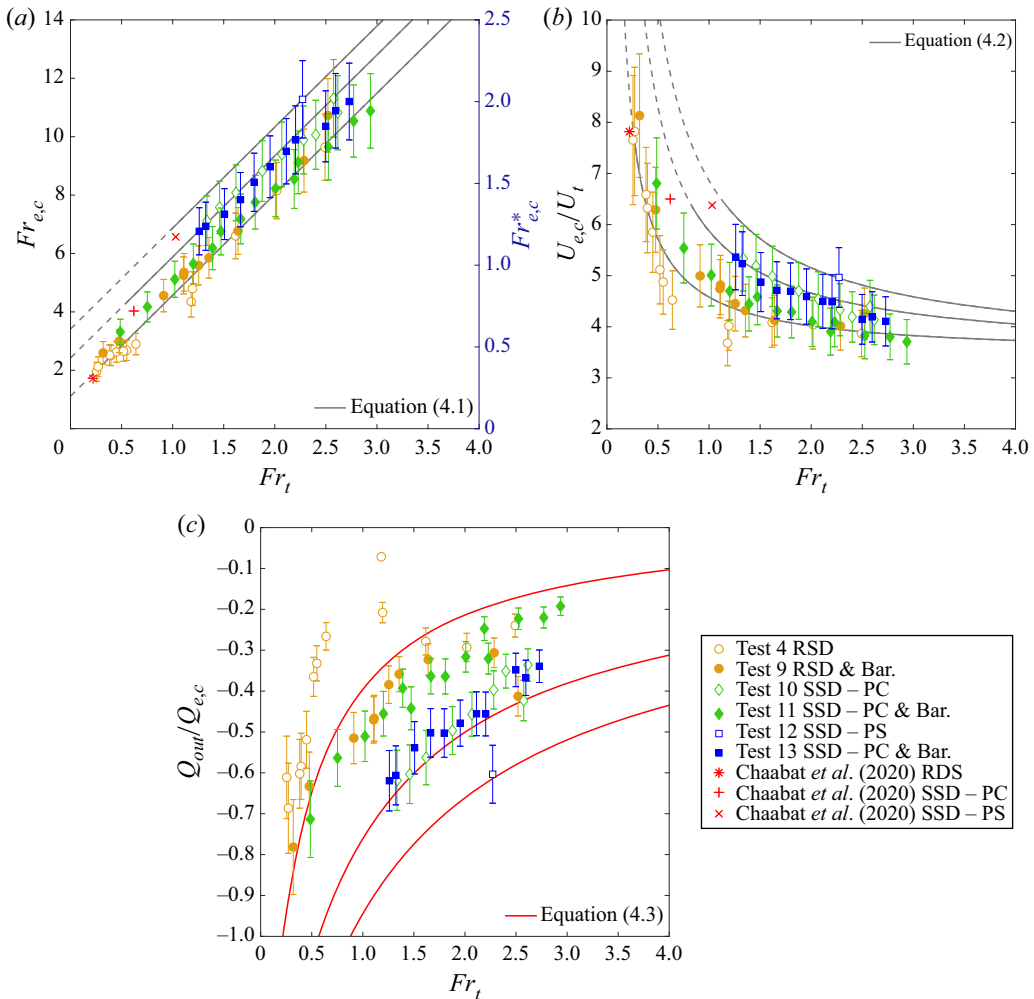


Figure 4. Variations in the aerodynamic behaviour of the ventilation system when different vent arrangements (hollow markers) and barriers (filled markers) are used in the experiments. In particular, the tunnel Froude number Fr_t as a function of (a) the extraction Froude number $Fr_{e,c}$, (b) the ratio between velocities $U_{e,c}/U_t$ and (c) the normalised outlet flow rate $Q_{out}/Q_{e,c}$, respectively, is given. In panels (a) and (b) the grey curves indicate (4.1) and (4.2) with different values of the fitting coefficient b , while the red curves display the analytical expression of (4.3). Furthermore, in panels (a,b), the data of Chaabat et al. (2020) are reported for comparison.

a slightly different criterion to determine the confinement conditions). Therefore, we can assert that a combined ventilation system, differently from a purely transverse one, allows for the obtainment of total confinement (i.e. $L/H = 0$) even with centred and off-centred squared dampers.

A possible way to improve the effectiveness of an existing ventilation system is the deployment of solid barriers in the tunnel ceiling in emergency situations. The main action of the barriers is to block the propagation of the gravity current generated by the buoyant release once impacted the tunnel ceiling (Chaabat et al., 2020). Furthermore, for longitudinal ventilation, their set-up improves the control of the back-layering length by locally increasing the longitudinal mean velocity in the tunnel cross-section (Chaabat et al., 2019), hence requiring a slower U_t with respect to the case of an empty tunnel. With a combined ventilation system, the barriers should guarantee both the aforementioned beneficial effects.

Tests 9, 11 and 13 (table 2), reported in figure 4(a,b), were conducted specifically to quantify the effect of the barriers on the flow. It can be appreciated that vertical barriers are effective, when used combined with square-shaped dampers, in reducing the extraction velocity required to impose confinement conditions, compared with the case of an empty tunnel. Instead, with RSD, the beneficial action of the barriers is limited or negligible (figure 4a), since their opening already spans the whole tunnel width (Chaabat et al., 2020). The effect of barriers with the square-shaped dampers can be summarised as follows (figure 4a,b): the SSD-PS with the barriers perform in a similar way as the SSD-PC without the presence of the barriers and, in turn, the SSD-PC behave as they were RSD, thanks to the disposition of the vertical barriers.

In figure 4(c), the experimental data are presented together with estimates given by (4.3), plotted adopting values of ρ_e/ρ_0 , ρ_s/ρ_0 , $Q_s/Q_{e,c}$ and b representative of different series of tests. For what concerns the flow rate within the tunnel, for increasing Fr_t , the ratio $Q_{out}/Q_{e,c}$ exhibits a shift, depending on the source morphology and the presence or absence of the barriers (figure 4c). As already noticed, the SSD-PS with the barriers and the SSD-PC without barriers behave similarly, but they tend towards a lower value of $Q_{out}/Q_{e,c}$ than the cases SSD-PC with barriers and RSD (both with and without barriers). In other words, for the same Fr_t , SSD-PS with the barriers and the SSD-PC without barriers produce a higher negative flow rate Q_{out} compared with the other cases (except for the SSD-PS without barriers that produce an even higher negative flow rate).

4.2. Flow regimes

In the experiments we could observe that, once confined within the two extraction fans, the buoyant fluid can achieve different stratification conditions. These are dictated by two competing mechanisms, namely the buoyancy effects that tend to stabilise and maintain the stratification, and the inertial forces that promote mixing within the flow (Yang et al., 2010). Based on the visualisations of the distribution of the buoyant flow, we could identify four different flow regimes (see figure 5). First of all, we clearly observe two limiting conditions:

- Regime I (figure 5a): the flow is stratified, with the light gas lying close to the tunnel ceiling, since the buoyancy effects prevail over turbulent mixing;
- regime IV (figure 5d): the buoyant fluid is present only downwind the source due to the overwhelming effect of the longitudinal velocity.

More subtle to identify, but nevertheless systematically observed, are two other regimes. These are associated with the rise of asymmetries of the flow with respect to the source and the progressive disruption of a clear boundary between the upper light layer and the fresh air below:

- Regime II (figure 5b): the buoyant fluid is unstratified on the upwind side, due to the growing role of Kelvin–Helmholtz instabilities, and stratified at the downwind side;
- regime III (figure 5c): the turbulent fluctuations overcome the density gradients, so that the light gas mixes with the ambient air, on both sides of the source.

As a first step, our focus is on the occurrence of flow regimes as a function of the two control parameters Fr_t and $Fr_{e,c}$ (or $Fr_{e,c}^*$), which we present in figure 6(a) for the RSD. Interestingly, we observe an almost perfect succession of the four regimes, as identified in figure 5, as both the longitudinal and extraction velocities increase. For values lower than $Fr_t \approx 0.54$ and $Fr_{e,c} \approx 3.07$, the flow is stably stratified (figure 5(a), regime I). For larger values of the Froude numbers, the flow becomes partly stratified (on the left side) and partly unstratified (on the right side), showing an intermediate condition (figure 5(b), regime II) as long as Fr_t and $Fr_{e,c}$ do not exceed the values of 0.96 and 4.48, respectively. When $Fr_t \gtrsim 1$ and $Fr_{e,c} \gtrsim 4.85$, the flow exhibits an unstratified flow regime (figure 5(c), regime III) and when the tunnel and the extraction Froude number overcome the thresholds equal to ≈ 1.30 and ≈ 5.70 , respectively, the buoyant fluid is completely pushed downwind the left vent by the longitudinal

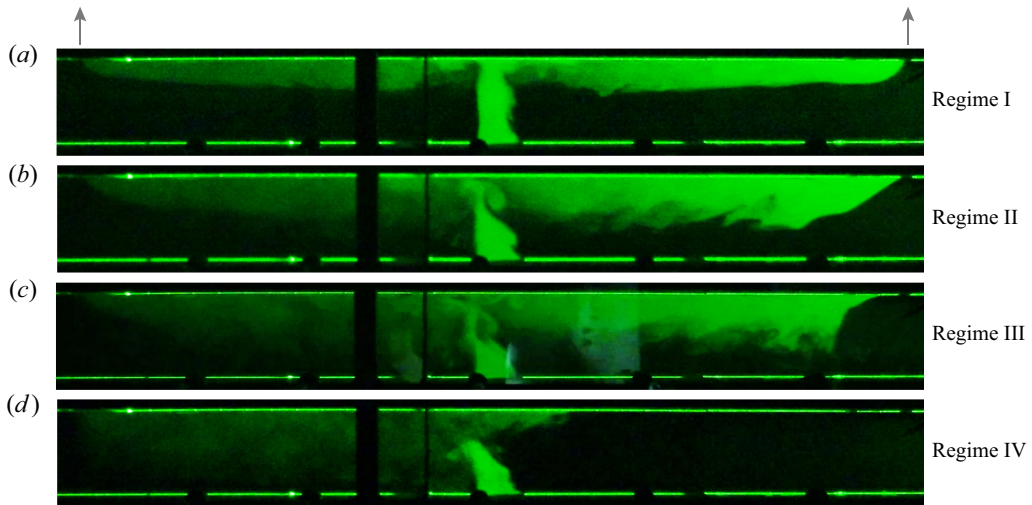


Figure 5. Examples of stratification conditions of the buoyant plume in the tunnel with rectangular dampers (RSD): (a) regime I – stratified flow; (b) regime II – intermediate condition, i.e. the flow is stratified at one side (left) and unstratified on the other side (right); (c) regime III – unstratified flow; (d) regime IV – condition with a strong longitudinal velocity. The grey arrows indicate the position of the vertical vents while the tips point in the direction of the transverse extraction.

flow (figure 5(d), regime IV). To better visualise these limits, we have qualitatively highlighted the occurrence of the different flow regimes with RSD by using a grey colour scale in figure 6(a).

The implementation of dampers with different shapes highly affects the buoyant flow regime (additionally evidenced in figure 6(b) through the grey colour scale that reports the limits individuated for the RSD as a benchmark). Indeed, placing both the SSD-PC and the SSD-PS prevents the occurrence of a stratified flow (regimes I and II), so that only regimes III and IV can actually occur. The situation can somehow be improved using the barriers. Both in the case of RSD and SSD-SP, the best and the worst vents, respectively, barriers have no major role in altering the flow regimes (figure 6b). We can instead observe a relevant effect for the SSD-PC (reported with hollow and filled diamonds in figure 6b). Indeed, the adoption of the barriers induces a significant reduction of the Froude number required to confine the buoyant release, which goes with a change of the respective flow regime, switching from the unstratified condition of regimes III and IV to the stratified condition of regime I.

5. Conclusions

By means of a flow visualisation technique, a series of experiments were carried out by releasing a light fluid (simulating the presence of a fire) within a tunnel with a rectangular cross-section and equipped with both longitudinal and transverse ventilation systems. Two ceiling extractor vents were located on each side of the plume source. The investigation encompassed different combinations of the source parameters as well as different geometrical configurations (rectangular and square shape) and arrangements (central and lateral) of the vents. The effect of the deployment of large fixed vertical barriers at the tunnel ceiling was also considered, by means of dedicated tests. We have focused on the flow conditions that allow the light gas release to be fully confined between two vertical vents, avoiding the formation of back-layering flows. The main outcomes can be summarised in the following points.

- (i) If the vent configuration is kept fixed (e.g. with rectangular-shaped vents), the only flow control parameters are the tunnel Froude number Fr_t and the extraction Froude number $Fr_{e,c}$, which are shown to be linked by a relationship of the form $Fr_{e,c} = aFr_t + b$. This implies that other parameters characterising the buoyant release, such as the plume Richardson number Γ_s and the

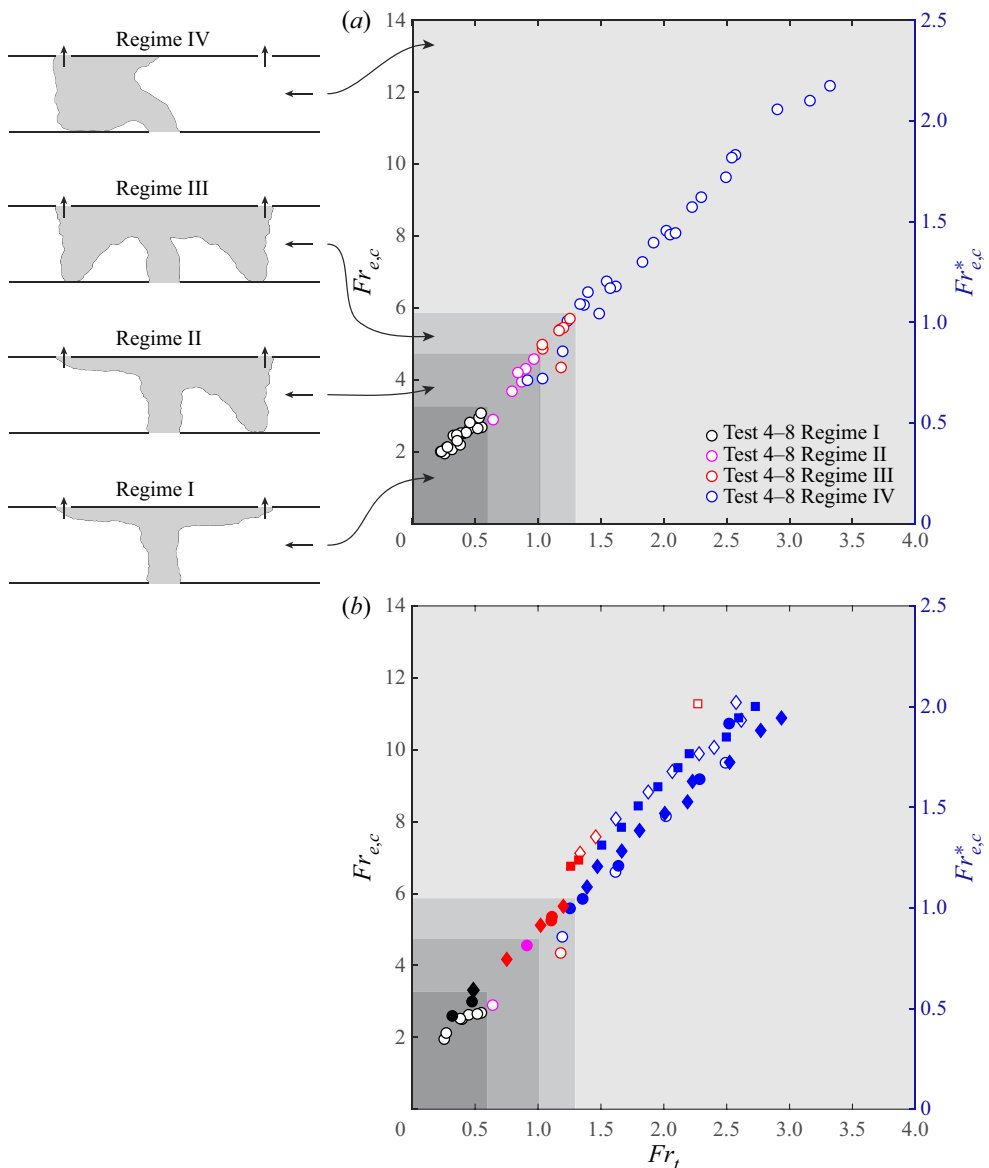


Figure 6. Flow regime of the buoyant plume with (a) rectangular dampers and (b) varying damper configurations. The marker type (circle, diamond and square) represents different vent shapes (RSD, SSD-PC and SSD-PS, for details, see the legend in figure 4), hollow/filled indicates the absence/presence of barriers (for details, see the legend in figure 4) while the marker colour indicates the flow regime. On the left, sketches depicting the different flow regimes are reported to help in the interpretation of the results.

density ratio ρ_s/ρ_0 , play a marginal role in the flow dynamics within the tunnel, as already observed for other ventilation systems (Chaabat et al., 2020; Jiang et al., 2018, 2019).

- (ii) In the tunnel stretch downstream of the vertical vents, the flow rate is directed in the opposite direction with respect to the longitudinal flow towards the dampers. This ‘suction effect’ progressively fades out for increasing the intensity of the imposed longitudinal flow. Therefore the ratio $Q_{out}/Q_{e,c}$ is reduced in magnitude for increasing Fr_t , approaching a constant value.

- (iii) Both the shape and the location of the dampers are pivotal parameters in controlling buoyant plumes in tunnels. Indeed, as pointed out by Chaabat et al. (2020) for a transverse ventilation system, using centred square dampers instead of rectangular dampers (which occupy the entire tunnel width), requires a higher longitudinal velocity (or a higher extraction velocity) to achieve confinement conditions. The situation is even worsened when off-centred square dampers are considered.
- (iv) The installation of vertical barriers with rectangular dampers does not improve the effectiveness in the confinement of the buoyant release. This is because the dampers and the barriers have the same width, hence the beneficial effect induced by the barriers is marginal. The situation in which the barriers are used in combination with centred and off-centred square dampers is different. In these circumstances, the presence of the barriers permits the dampers to make a qualitative leap: with the barriers, the off-centred square dampers work as the centred square dampers in empty tunnels and, in turn, centred square dampers have the same performance as the rectangular dampers. This is due to the fact that the buoyant back-layer flow is blocked by the barrier and channelled towards the vent.
- (v) The confined buoyant plume can exhibit four distinct flow regimes, i.e. stratified (regime I), intermediate condition (regime II), unstratified (regime III) or an extreme condition where the plume is deviated by the strong longitudinal velocity towards the downstream vent (regime IV). With rectangular dampers, if $Fr_t \lesssim 0.54$ and $Fr_{e,c} \lesssim 3.07$, the buoyant plume is stratified while if $Fr_t \gtrsim 1$ and $Fr_{e,c} \gtrsim 4.85$ the buoyant flow first becomes unstratified and then, for even greater values of Fr_t and $Fr_{e,c}$, the plume moves entirely towards the downstream damper. In this condition ($Fr_t \gtrsim 2$), the role of buoyancy on the flow dynamics becomes marginal and the velocity ratio $U_{e,c}/U_t$ tends to a constant value. With different damper shapes and positions, the buoyant plume can be confined only in unstratified conditions. Also with regard to the stratification conditions, the use of barriers is effective only for the case of centred square dampers and allows for a switch toward regime I.

These results provide important information for combined ventilation system design and management, reporting the drawbacks and potentiality of using different vent shapes and positions as well as large vertical barriers.

Acknowledgements. The authors are grateful to the assistant-engineer H. Correia (LMFA) for the technical aid in the realisation of the experimental set-up.

Declaration of interests. The authors declare no conflict of interest.

Funding statement. This work was supported by the Région Auvergne-Rhône-Alpes (France) within the COVENTU Project (grant number: GFC 2020-043).

Author contributions. M.M. and P.C. designed, performed all measurements and pre-processed the data. C.P. processed, analysed the data and wrote the manuscript, with supervision from P.S. Lastly, D.A., T.K. and A.M. gave useful comments and revised the manuscript.

Data availability statement. Raw data are available from the corresponding author.

Ethical standards. The research meets all ethical guidelines, including adherence to the legal requirements of the study country.

References

- Alva, W.U.R., Jomaas, G., & Dederichs, A.S. (2017). The influence of vehicular obstacles on longitudinal ventilation control in tunnel fires. *Fire Safety Journal*, 87, 25–36.
- Arya, S.P.S., & Lape, J.F.J. (1990). A comparative study of the different criteria for the physical modeling of buoyant plume rise in a neutral atmosphere. *Atmospheric Environment. Part A. General Topics*, 24(2), 289–295.
- Bai, J., Liao, H., & Xia, Y. (2020). Study on fire accidents in tunnels. In *IOP conference series: Materials science and engineering* (vol. 741, p. 012095). Chongqing, China: IOP Publishing.
- Barenblatt, G.I. (1996). *Scaling, self-similarity, and intermediate asymptotics: Dimensional analysis and intermediate asymptotics*. Cambridge, UK: Cambridge University Press.
- Brousse, B., Voeltzel, A., Le Botlan, Y., & Ruffin, E. (2002). Mont Blanc tunnel ventilation and fire tests. *Tunnel Management International*, 5(1), 13–22.

- Carlotti, P., Vallerent, S., Fromy, P., & Demouge, F. (2012). Smoke motion: Comparison of experimental data with simulations. *Proceedings of the Institution of Civil Engineers: Engineering and Computational Mechanics*, 165(4), 235–244.
- Carvel, R., & Marlair, G. (2005). A history of fire incidents in tunnels. In *The handbook of tunnel fire safety* (pp. 1–41). London, UK: Thomas Telford.
- Chaabat, F., Creyssels, M., Mos, A., Wingrave, J., Correia, H., Marro, M., & Salizzoni, P. (2019). The effects of solid barriers and blocks on the propagation of smoke within longitudinally ventilated tunnels. *Building and Environment*, 160, 106207.
- Chaabat, F., Salizzoni, P., Creyssels, M., Mos, A., Wingrave, J., Correia, H., & Marro, M. (2020). Smoke control in tunnel with a transverse ventilation system: An experimental study. *Building and Environment*, 167, 106480.
- Chen, L.F., Hu, L.H., Zhang, X.L., Zhang, X.Z., Zhang, X.C., & Yang, L.Z. (2015). Thermal buoyant smoke back-layering flow length in a longitudinal ventilated tunnel with ceiling extraction at difference distance from heat source. *Applied Thermal Engineering*, 78, 129–135.
- Cingi, P., Angeli, D., Cavazzuti, M., Levoni, P., Stalio, E., & Cipollone, M. (2021). An integrated approach for the analysis and modeling of road tunnel ventilation. Part II: Numerical model and its calibration. *Transportation Engineering*, 4, 100063.
- Danziger, N.H., & Kennedy, W.D. (1982). Longitudinal ventilation analysis for the Glenwood canyon tunnels. In *4th international symposium on aerodynamics & ventilation of vehicle tunnels, March 23–25, York, UK* (pp. 169–186).
- Drysdale, D. (2011). *An introduction to fire dynamics* (3rd ed.). Chichester, UK: John Wiley & Sons.
- European Commission (2004). *Directive 2004/54/EC of the European parliament and of the council on minimum safety requirements for tunnels in the Trans-European road network*. Brussels, Belgium: Official Journal of the European Union.
- Ezzamel, A., Salizzoni, P., & Hunt, G.R. (2015). Dynamical variability of axisymmetric buoyant plumes. *Journal of Fluid Mechanics*, 765, 576–611.
- Fridolf, K., Nilsson, D., & Frantzich, H. (2013). Fire evacuation in underground transportation systems: A review of accidents and empirical research. *Fire Technology*, 49(2), 451–475.
- Grant, G.B., Jagger, S.F., & Lea, C.J. (1998). Fires in tunnels. *Philosophical Transactions of the Royal Society A*, 356(1748), 2873–2906.
- Halawa, T., & Safwat, H. (2021). Fire-smoke control strategies in road tunnels: The effectiveness of solid barriers. *Case Studies in Thermal Engineering*, 27, 101260.
- He, L., Xu, Z., Chen, H., Liu, Q., Wang, Y., & Zhou, Y. (2018). Analysis of entrainment phenomenon near mechanical exhaust vent and a prediction model for smoke temperature in tunnel fire. *Tunnelling and Underground Space Technology*, 80, 143–150.
- He, L., Xu, Z., Markert, F., Zhao, J., Liu, Q., Tao, H., Wang, Z., & Fan, C. (2020). Experimental study of heat exhaust efficiency with natural ventilation in tunnel fire: Impact of shaft height and heat release rate. *Journal of Wind Engineering and Industrial Aerodynamics*, 201, 104173.
- Herning, F., & Zipperer, L. (1936). Calculation of the viscosity of technical gas mixtures from the viscosity of the individual gases. *Gas und Wasserfach*, 79, 69.
- Heskestad, G. (1998). Dynamics of the fire plume. *Philosophical Transactions of the Royal Society A*, 356(1748), 2815–2833.
- Hu, L.H., Huo, R., & Chow, W.K. (2008). Studies on buoyancy-driven back-layering flow in tunnel fires. *Experimental Thermal and Fluid Science*, 32(8), 1468–1483.
- Hunt, G.R., & Kaye, N.B. (2005). Lazy plumes. *Journal of Fluid Mechanics*, 533, 329–338.
- Ingason, H., & Li, Y.Z. (2010). Model scale tunnel fire tests with longitudinal ventilation. *Fire Safety Journal*, 45(6–8), 371–384.
- Jiang, L., Creyssels, M., Hunt, G.R., & Salizzoni, P. (2019). Control of light gas releases in ventilated tunnels. *Journal of Fluid Mechanics*, 872, 515–531.
- Jiang, L., Creyssels, M., Mos, A., & Salizzoni, P. (2018). Critical velocity in ventilated tunnels in the case of fire plumes and densimetric plumes. *Fire Safety Journal*, 101, 53–62.
- Jiang, L., & Ingason, H. (2020). Use of mobile fans during tunnel fires. *Tunnelling and Underground Space Technology*, 106, 103618.
- Joint Committee for Guides in Metrology (2008). *Evaluation of measurement data — guide to the expression of uncertainty in measurement* (vol. 100). Sèvres, France: JCGM.
- Kubwimana, T. (2020). *Simulation de l'écoulement atmosphérique au voisinage d'une tête de tunnel* (PhD thesis). École Centrale de Lyon.
- Kubwimana, T., Salizzoni, P., Bergamini, E., Mos, A., Méjean, P., & Soulhac, L. (2018). Wind-induced pressure at a tunnel portal. *Environmental Fluid Mechanics*, 18(3), 769–786.
- Le Clanche, J., Salizzoni, P., Creyssels, M., Mehaddi, R., Candelier, F., & Vauquelin, O. (2014). Aerodynamics of buoyant releases within a longitudinally ventilated tunnel. *Experimental Thermal and Fluid Science*, 57, 121–127.
- Lee, E.J., Oh, C.B., Oh, K.C., Yoo, Y.H., & Shin, H.J. (2010). Performance of the smoke extraction system for fires in the Busan–Geoje immersed tunnel. *Tunnelling and Underground Space Technology*, 25(5), 600–606.
- Leitner, A. (2001). The fire catastrophe in the Tauern Tunnel: Experience and conclusions for the Austrian guidelines. *Tunnelling and Underground Space Technology*, 16(3), 217–223.
- Levoni, P., Angeli, D., Cingi, P., Barozzi, G.S., & Cipollone, M. (2021). An integrated approach for the analysis and modeling of road tunnel ventilation. Part I: Continuous measurement of the longitudinal airflow profile. *Transportation Engineering*, 3, 100039.
- Levoni, P., Angeli, D., Stalio, E., Agnani, E., Barozzi, G.S., & Cipollone, M. (2015). Fluid-dynamic characterisation of the Mont Blanc tunnel by multi-point airflow measurements. *Tunnelling and Underground Space Technology*, 48, 110–122.

- Li, J.S.M., & Chow, W.K. (2003). Numerical studies on performance evaluation of tunnel ventilation safety systems. *Tunnelling and Underground Space Technology*, 18(5), 435–452.
- Li, Y.Z., Lei, B., & Ingason, H. (2010). Study of critical velocity and backlayering length in longitudinally ventilated tunnel fires. *Fire Safety Journal*, 45(6–8), 361–370.
- Linden, P.F. (2000). Convection in the environment. In *Perspectives in fluid dynamics: A collective introduction to current research* (ed. G.K. Batchelor, H.K. Moffatt & M.G. Worster), vol. 289, p. 343. Cambridge, UK: Cambridge University Press.
- Liu, Y., & Yang, D. (2022). Effects of baffles on heat and contaminant removal for tunnel smoke extraction: Evaluation criteria regarding removal efficiency and flow resistance. *Case Studies in Thermal Engineering*, 32, 101887.
- Lovas, S., Carlotti, P., Desanghère, S., & Mos, A. (2011). Optimization of the repartition of extraction vents in transverse ventilation. In *14th international symposium on aerodynamics & ventilation of tunnels, May 11–13, Dundee, UK*.
- Marjanovic, G., Taub, G.N., & Balachandar, S. (2017). On the evolution of the plume function and entrainment in the near-source region of lazy plumes. *Journal of Fluid Mechanics*, 830, 736–759.
- Morton, B.R. (1959). Forced plumes. *Journal of Fluid Mechanics*, 5(1), 151–163.
- Morton, B.R., Taylor, G.I., & Turner, J.S. (1956). Turbulent gravitational convection from maintained and instantaneous sources. *Proceedings of the Royal Society A*, 234(1196), 1–23.
- Nironi, C., Salizzoni, P., Marro, M., Mejean, P., Grosjean, N., & Soulhac, L. (2015). Dispersion of a passive scalar fluctuating plume in a turbulent boundary layer. Part I: Velocity and concentration measurements. *Boundary-Layer Meteorology*, 156(3), 415–446.
- Oucherfi, M., Gay, B., Mos, A., & Carlotti, P. (2009). Definition and optimisation of the efficiency of smoke extraction in a road tunnel. In *13th international symposium on aerodynamics & ventilation of vehicle tunnels, May 13–15, New Brunswick, NJ*.
- PIARC Committee on Road Tunnels (1999). *Fire and smoke control in road tunnels*, vol. 05.05.BEN. Puteaux, France: PIARC.
- Ren, R., Zhou, H., Hu, Z., He, S., & Wang, X. (2019). Statistical analysis of fire accidents in Chinese highway tunnels 2000–2016. *Tunnelling and Underground Space Technology*, 83, 452–460.
- Salizzoni, P., Creyssels, M., Jiang, L., Mos, A., Mehaddi, R., & Vauquelin, O. (2018). Influence of source conditions and heat losses on the upwind back-layering flow in a longitudinally ventilated tunnel. *International Journal of Heat and Mass Transfer*, 117, 143–153.
- Seike, M., Kawabata, N., & Hasegawa, M. (2014). The effect of fixed smoke barriers on evacuation environment in road tunnel fires with natural ventilation. In *7th international conference 'tunnel safety and ventilation', May 12–13, Graz, Austria* (pp. 126–132).
- Tang, F., He, Q., Mei, F., Wang, Q., & Zhang, H. (2018). Effect of ceiling centralized mechanical smoke exhaust on the critical velocity that inhibits the reverse flow of thermal plume in a longitudinal ventilated tunnel. *Tunnelling and Underground Space Technology*, 82, 191–198.
- Tang, F., Li, L.J., Dong, M.S., Wang, Q., Mei, F.Z., & Hu, L.H. (2017). Characterization of buoyant flow stratification behaviors by Richardson (Froude) number in a tunnel fire with complex combination of longitudinal ventilation and ceiling extraction. *Applied Thermal Engineering*, 110, 1021–1028.
- Tang, F., Li, L.J., Mei, F.Z., & Dong, M.S. (2016). Thermal smoke back-layering flow length with ceiling extraction at upstream side of fire source in a longitudinal ventilated tunnel. *Applied Thermal Engineering*, 106, 125–130.
- Tao, L., & Zeng, Y. (2022). Effect of different smoke vent layouts on smoke and temperature distribution in single-side multi-point exhaust tunnel fires: A case study. *Fire*, 5(1), 28.
- Thomas, P.H. (1958). The movement of buoyant fluid against a stream and the venting of underground fires. *Fire Safety Science*, 351, 1–7.
- Thomas, P.H. (1968). The movement of smoke in horizontal passages against an air flow. In *Fire research station report* (pp. 1–6). Fire Research Note 723.
- Vauquelin, O. (2008). Experimental simulations of fire-induced smoke control in tunnels using an 'air-helium reduced scale model': Principle, limitations, results and future. *Tunnelling and Underground Space Technology*, 23(2), 171–178.
- Vauquelin, O., Michaux, G., & Lucchesi, C. (2009). Scaling laws for a buoyant release used to simulate fire-induced smoke in laboratory experiments. *Fire Safety Journal*, 44(4), 665–667.
- Vauquelin, O., & Wu, Y. (2006). Influence of tunnel width on longitudinal smoke control. *Fire Safety Journal*, 41(6), 420–426.
- Vidal, C., Marro, M., Correia, H., Gostiaux, L., Jallais, S., Houssin, D., Vyazmina, E., & Salizzoni, P. (2022). Wind-tunnel experiments on atmospheric heavy gas dispersion: metrological aspects. *Experimental Thermal and Fluid Science*, 130, 110495.
- Vuilleumier, F., Weatherill, A., & Crausaz, B. (2002). Safety aspects of railway and road tunnel: example of the Lötschberg railway tunnel and Mont-Blanc road tunnel. *Tunnelling and Underground Space Technology*, 17(2), 153–158.
- Wang, J., Yuan, J., Fang, Z., Tang, Z., Qian, P., & Ye, J. (2018). A model for predicting smoke back-layering length in tunnel fires with the combination of longitudinal ventilation and point extraction ventilation in the roof. *Tunnelling and Underground Space Technology*, 80, 16–25.
- Yang, D., Hu, L.H., Huo, R., Jiang, Y.Q., Liu, S., & Tang, F. (2010). Experimental study on buoyant flow stratification induced by a fire in a horizontal channel. *Applied Thermal Engineering*, 30(8–9), 872–878.
- Yao, Y., Cheng, X., Zhang, S., Zhu, K., Shi, L., & Zhang, H. (2016). Smoke back-layering flow length in longitudinal ventilated tunnel fires with vertical shaft in the upstream. *Applied Thermal Engineering*, 107, 738–746.

Zhu, Y., Tang, F., Chen, L., Wang, Q., & Xu, X. (2020). Effect of lateral concentrated smoke extraction on the smoke back-layering length and critical velocity in a longitudinal ventilation tunnel. *Journal of Wind Engineering and Industrial Aerodynamics*, 207, 104403.

Cite this article: Salizzoni P, Peruzzi C, Marro M, Cingi P, Angeli D, Kubwimana T, Mos A (2023). Measurements and scaling of buoyancy-induced flows in ventilated tunnels. *Flow*, 3, E15. doi:10.1017/flo.2023.10